High-resolution x-ray spectrum of a laser-produced barium plasma in the 9.10–9.36-Å wavelength range

R. Doron, E. Behar, M. Fraenkel, P. Mandelbaum, A. Zigler, and J. L. Schwob
Racah Institute of Physics, The Hebrew University, 91904 Jerusalem, Israel

A. Ya. Faenov and T. A. Pikuz
Multicharged Ion Spectra Data Center, VNIIFTRI, Mendelèevo, Moscow Region 141570, Russia

(Received 7 November 1997)

A highly stripped barium plasma is produced by 120-fs laser pulses irradiating a BaF_2 target. The spectrum emitted by the plasma in the 9.10–9.36-Å wavelength range is recorded using a high-resolution spherically bent mica crystal. On the basis of the HULLAC atomic code, a level-by-level collisional-radiative model including autoionization and dielectronic capture processes is developed to calculate the wavelengths and intensities of the spectral lines emitted by each of the Cu-, Zn-, and Ga-like barium ions. $3d$-nf ($n=6,7$) spectral lines with different spectator electrons, previously observed only as unresolved transition arrays, are resolved. The theoretical results agree reasonably well with experiment. Best agreement is obtained for electron density and temperature of 5×10^{21} cm^{-3} and 120 eV, respectively. The intensity ratios of the resolved Cu-like barium lines are shown to be useful tools for electron density and temperature diagnosis. This diagnostic method was not possible with low-resolution spectroscopy. It is found that at relatively low temperature and high density as in the present experiment, the *relative* intensities of lines within each ionization state are independent of the ion density ratio of adjacent ionization states.

[S1050-2947(98)01209-8]

PACS number(s): 32.30.Rj, 32.70.−n, 52.70.−m

I. INTRODUCTION

The research on plasmas of highly ionized heavy elements produced by subpicosecond lasers irradiating solid targets has greatly progressed in the last few years. Recent improvement in laser power densities together with the development of very high resolution x-ray crystal spectrometers have provided new insights into the nature of such plasmas. Still, many of the characteristics of these plasmas are believed to be strongly dependent upon the time and space profile of the laser pulse and are yet to be fully understood. Specifically for barium, an experiment with powerful ultrashort laser pulses irradiating on barium compound targets was already performed by Zigler *et al.* [1], and the emitted x-ray spectrum was recorded. This spectrum was analyzed by Goldstein *et al.* [2] in the framework of the local thermodynamic equilibrium (LTE) model. Recently, another experiment for measuring x-ray emission from a laser-produced barium plasma over a relatively wide wavelength range from 8 to 14 Å has been carried out [3]. The spectrum was found to consist mainly of unresolved transition arrays (UTA) emitted by Fe- to Ge-like barium ions.

In the present work, we present a different measurement of the same x-ray emission using a spherically bent mica crystal [4] with very high spectral resolution, which enables better insight into the unresolved spectral features. The mica crystal technique has already proven to be a powerful tool for spectroscopic investigations [5,6]. The price for the high resolution is the limited spectral region, which in the present case is 9.10–9.36 Å. This wavelength range corresponds mainly to the $3d$-$6f$ transitions of Cu- and Zn-like barium, and to the $3d$-$7f$ transitions of Ga-like barium [3]. In addition to the precise wavelength measurements, the highly resolved spectrum allows the identification of new lines and opens possibilities for new plasma diagnostic methods.

The plasma investigated in Refs. [1] and [2] was produced by intense 650-fs laser pulses of power density 10^{17} W/cm^2 at a wavelength of 0.248 μm. Transparent BaF_2 targets were used to eliminate the prepulse effect. The x-ray spectrum was recorded and identified as $3d$-$4f$ transitions emitted by Sc- to Ni-like barium. The spectrum showed strong continuum features and therefore was modeled using the super transition array (STA) theory [7] assuming an optically thin LTE plasma. The STA model indicated near solid density, and a weighted electron temperature distribution of seven different temperatures in the 200–350-eV range was assumed in order to reproduce the space- and time-integrated experimental spectrum.

In the present experiment, although the targets are also BaF_2, the laser wavelength is much longer, the pulse duration is much shorter, and the laser power density is somewhat lower. The analysis of the present spectrum clearly indicates that at least the part of the plasma emitting the $3d$-nf ($n=6,7$) lines departs from the pure LTE regime. Therefore, here one must construct a detailed collisional-radiative model. Since the upper levels of the $3d$-nf radiative transitions are autoionizing, the model includes autoionization and dielectronic capture processes.

The intensities of spectral lines arising from autoionizing levels can strongly depend upon the plasma electron density n_e and temperature T_e. Therefore, these lines are candidates for plasma diagnostic tools. Particularly, the use of $3d$-nf ($n=4,5$) lines emitted by ions isoelectronic to CuI, ZnI, and GaI, where the upper levels are autoionizing, has been suggested by Bauche-Arnoult *et al.* [8] and by Mandelbaum *et al.* [9] for diagnostic purposes. In the present work, $3d$-$6f$ lines, emitted by Cu-like barium with different electron spectators, are employed. For fully modeling the plasma and the

spectrum emitted by ions in autoionizing levels it is necessary to know the relative abundances of neighboring ionization states. However, in transient plasmas with strong temperature and density gradients such as the present plasma, the ion abundance ratios vary as a function of space and time. Moreover, in the case of *dielectronic recombination* spectra, the line intensities depend upon the abundance ratio of two ionization states that cannot be easily determined experimentally. Therefore, these ratios are taken here as free parameters in the model.

II. EXPERIMENTAL SETUP

The plasma is generated by the irradiation of intense ultrashort laser pulses on solid BaF_2 targets. The laser generates 20-mJ, 120-fs pulses at a repetition rate of 10 Hz. This laser is based on a Ti:sapphire oscillator generating 80-fs pulses at a wavelength of 0.800 μm with a spectral width of about 10 nm. The 80-fs pulses are amplified by the chirped pulse amplification (CPA) technique [10] in which they are first stretched temporarily to a width of about 1 ns, subsequently sent into a regenerative amplifier and a double-pass amplifier, and finally recompressed to a pulse width of 120 fs. The laser pulse is focused on the BaF_2 target to a focal spot of 20 μm, producing a laser power density of 5×10^{16} W/cm^2.

The x rays are dispersed by a high resolution ($\lambda/\Delta\lambda=10\,000$) spherical mica crystal [4], and the spectrum is recorded on Kodak Direct Exposure film shielded by a visible light absorber. The positions of the spectral lines on the photographic films are measured both by means of a Grant comparator and also by digitally scanning the films using a high optical density and high resolution charge-coupled device. The Grant comparator has a higher spatial resolution, whereas the scanner gives more reliable line intensities. Only spectra recorded by the scanner are shown in this paper. The accuracy of the wavelength measurement, based on recent high-resolution measurements of He- and Li-like Mg reference lines [5], is estimated to be about 0.9 mÅ. In addition, the radiation emitted by the plasma is simultaneously dispersed by a flat RAP crystal for which the absolute intensities can be derived by introducing accurate corrections to account for film sensitivity [11], crystal efficiency [12], filter transmission, and source to film distance.

III. THEORETICAL MODEL

A collisional-radiative model is constructed to describe the spectral line intensities based on the level populations of the relevant Ba ions. Three separate models are built for describing the Cu-, Zn-, and Ga-like dielectronic recombination emission, including 3955, 4019, and 1803 levels, respectively. In each model only two adjacent ionization states are considered taking the density ratio $n_{\mathrm{Ni\,I}}/n_{\mathrm{Cu\,I}}$, $n_{\mathrm{Cu\,I}}/n_{\mathrm{Zn\,I}}$, or $n_{\mathrm{Zn\,I}}/n_{\mathrm{Ga\,I}}$ as a free parameter. Here n_x represents the number density of barium ions in all levels of a given ionization state x, excluding the population of doubly excited ions, which was found to be relatively small. Since the spectrum is time integrated and the time evolution of the plasma is not well known, a steady-state model is employed. The plasma is assumed to be optically thin. The procedure carried out is as follows: first, the populations of the *singly excited* levels are found by solving two separate sets of rate equations: one for the emitting ion (e.g., Cu-like $3d^{10}nl$) and one for the next ionized ion (e.g., Ni-like $3d^{10}$ and $3d^9 4l$). These equations can be written as

$$\frac{dn_i}{dt}=n_e\sum_{j\neq i}n_jQ_{ji}(T_e)+\sum_{j>i}n_jA_{ji}-n_i\left(n_e\sum_{j\neq i}Q_{ij}(T_e)+\sum_{j<i}A_{ij}\right)=0. \tag{1}$$

n_i and n_j represent the density of ions in singly excited levels i and j, respectively, and n_e represents the electron density. A_{ji} denotes the Einstein coefficient for radiative decay from j to i, and $Q_{ij}(T_e)$ denotes the rate coefficient for collisional excitation or deexcitation.

In the second step, the populations of the *doubly* (or inner-shell) *excited* levels d (or d') of the emitting ion are calculated. The doubly excited configurations that are relevant to the x-ray emission in the wavelength range of the present experiment and that have been included here are $3d^9nl6f$ ($n=4,5$) and $3p^53d^{10}4l5s$ for the Cu-like ion, $3d^94snl6f$ ($n=4,5$) and $3p^53d^{10}4s4l5s$ for the Zn-like ion, and $3d^94s^24l7f$ for the Ga-like ion. The levels of these configurations are the upper levels of the main radiative transitions observed in the present spectrum. Other close configurations that mix strongly with the above configurations are included as well. However, in the Zn I and Ga I cases, some of the configuration mixings are not included due to computation limitations. Therefore, the results for these ionization states may be slightly less accurate than those for Cu I. In order to further improve the predictions of the model, the most important radiative decays to *lower* doubly excited configurations, for example $3d^94l4l'$ and $3d^94l5d$ in the Cu-like case, are also taken into account. In addition, the model includes transitions from and to the singly excited levels i of the emitting ion and the singly excited levels k of the next ionization state, using the populations of these levels found from solving Eq. (1). The populations of the levels k belonging to the next ionization state are normalized with respect to those of the levels i of the emitting ion according to the ion density ratio parameter (e.g., $n_{\mathrm{Ni\,I}}/n_{\mathrm{Cu\,I}}$). The steady-state collisional-radiative set of rate equations for levels d can be written as follows:

$$\begin{aligned}\frac{dn_d}{dt}=&n_e\sum_{d'\neq d}n_{d'}Q_{d'd}(T_e)+\sum_{d'>d}n_{d'}A_{d'd}\\&-n_d\left(n_e\sum_{d'\neq d}Q_{dd'}(T_e)+\sum_{d'<d}A_{dd'}\right)\\&+n_e\left(\sum_i n_iQ_{id}(T_e)+\sum_k n_k\beta^c_{kd}(T_e)\right.\\&\left.+n_e\sum_k n_k\beta^{\mathrm{TB}}_{kd}(T_e)\right)\\&-n_d\left(n_e\sum_i Q_{di}(T_e)+\sum_k A^a_{dk}\right.\\&\left.+n_e\sum_k S_{dk}(T_e)+\sum_i A_{di}\right)=0.\end{aligned} \tag{2}$$

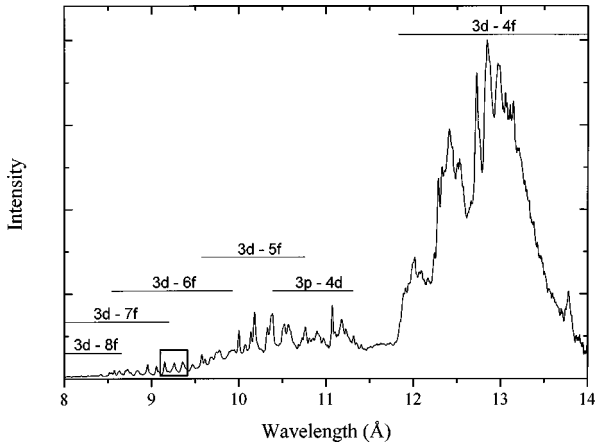

FIG. 1. X-ray spectrum of the laser-produced barium plasma in the 8–14-Å wavelength range obtained using a flat RAP crystal. The ranges of the transitions of the Cu-like and neighboring ionization states are given above the spectrum. The small square in the $3d$-$6f$ range indicates the spectral region investigated in the present work.

$\beta^c_{kd}(T_e)$ is the rate coefficient for dielectronic capture from k to d and A^a_{dk} is the rate coefficient for the reverse process, i.e., autoionization from d to k. $\beta^{\mathrm{TB}}_{kd}(T_e)$ is the rate coefficient for three-body recombination from k to d and $S_{dk}(T_e)$ is the rate coefficient for the reverse process, i.e., collisional ionization from d to k. Radiative recombination has been neglected. Finally, the populations of the levels d obtained by solving Eq. (2) are used for calculating the line intensities I_{di} arising from decays from the doubly excited levels d to singly excited levels i:

$$I_{di} = n_d A_{di} . \tag{3}$$

All lines are assumed here to have a uniform Gaussian profile.

The atomic quantities (energy levels, autoionization, radiative, and collisional rate coefficients) in the present work are calculated using the multiconfiguration relativistic HULLAC (Hebrew University Lawrence Livermore Atomic Code) computer package [13].

IV. SPECTROSCOPIC ANALYSIS

Figure 1 shows the whole range of the recorded spectrum, which was dispersed by the flat RAP crystal. Most of the spectral features seen in the figure were identified in Ref. [3]. The present work focuses on the limited wavelength range of 9.10–9.36 Å indicated in Fig. 1 by the small square. The x-ray spectrum emitted by the barium plasma in the present limited range is shown in Fig. 2 where the high-resolution recording obtained using the spherical mica crystal [Fig. 2(a)] is compared to the flat RAP crystal recording [Fig. 2(b)] in the same wavelength region. The spectral features observed using the RAP crystal have been recently identified [3] as $3d$-nf ($n=6,7$) UTA's. These identifications are given above the spectrum in Fig. 2(b). It is clearly seen that the use of the curved mica crystal spectrometer reveals new details of the spectrum, unobservable with lower resolution spectroscopy. The features that appear to be single broad

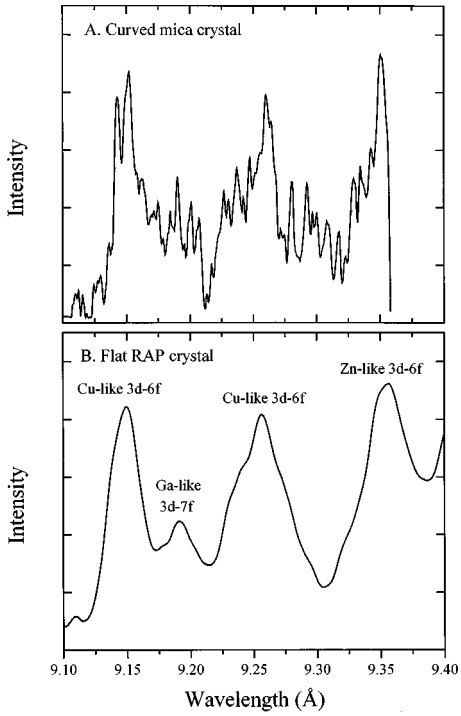

FIG. 2. X-ray spectrum of the laser-produced barium plasma in the 9.10–9.36-Å wavelength range. The upper trace (a) is a recording of the spectrum obtained with the spherical mica crystal, and the lower trace (b) is obtained with the flat RAP crystal. The UTA identifications from Ref. [3] are given in the lower trace above the spectrum.

UTA's in Fig. 2(b) are actually seen in Fig. 2(a) to be composed of many narrow lines that are coalesced into wide arrays in Fig. 2(b) due only to the instrumental broadening of the flat crystal technique. The high spectral resolution makes the line identification possible and consequently allows plasma diagnostics as described below.

It is found that thousands of Cu-, Zn-, and Ga-like computed lines arising from $3d$-nf ($n=6,7$) transitions with different electron spectators fall in the small wavelength region seen in Fig. 2. Thus, in order to identify the resolved peaks (about twenty) of the spectrum in Fig. 2(a), a straightforward comparison between computed and measured line wavelengths is insufficient, and it is necessary to model the line intensities using the collisional-radiative model described above. In Fig. 3 the theoretical spectrum obtained by modeling the Cu-, Zn-, and Ga-like line wavelengths and intensities is compared to the high-resolution experimental spectrum. All lines are given a uniform Gaussian profile of about 0.9 mÅ full width at half maximum (FWHM) to match the narrowest experimental linewidths. These widths are partially due to the instrumental resolution of the spectrometer and of the digital scanner. The relative line intensities emitted within each ionization state are directly obtained from the model, whereas the relative intensities of lines from different ionization states are normalized to fit the experimental spectrum. In order to improve the agreement with experiment and confirm the line identification, the theoretical wavelengths of all the lines belonging to a given ionization state have been slightly shifted by a constant value in Fig. 3. These shifts are of about 20 mÅ or less. In fact, using the parametric potential method [14] employed in the HULLAC code, one indeed

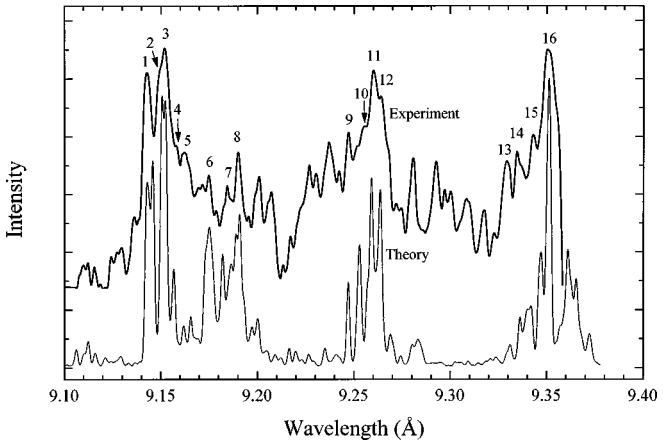

FIG. 3. Experimental spectrum of highly ionized barium in the 9.10–9.36-Å wavelength range obtained by the spherical mica crystal compared to the theoretical spectrum calculated for $n_e=5\times10^{21}$ cm^{-3} and $kT_e=120$ eV. Labels correspond to the transition identifications in Table I.

expects the inaccuracy in the theoretical wavelengths to be the same within each ionization state and to vary between different ionization states. This is a consequence of the energy levels being calculated separately for each ionization state. In order to obtain the best results, the calculations of the various ionization states are performed with different parametric potentials which are each obtained by a variational procedure. The theoretical spectrum fits the experimental results fairly well. It should be stressed that for the purpose of identifying the spectrum only features that were reproducible in several experimental spectra have been taken into account. This is one of the reasons for some of the weak unlabeled peaks in Fig. 3. It is found that the theoretical spectrum fits the experimental results best when the electron density and temperature are set to be 5×10^{21} cm^{-3} and 120 eV, respectively. These are the plasma parameters used for the theoretical spectrum shown in Fig. 3. A detailed discussion of the plasma diagnostic methods that lead to these parameter values is given in Sec. V.

The comparison of the experimental and theoretical spectra has allowed the identification of most of the observed peaks, which are labeled in Fig. 3. The line identifications are presented in Table I. The line labels are given in the first column. The next two columns show the measured wavelengths in angstroms [λ_{expt}(Å)] and the isoelectronic sequence of the emitting barium ion. Then, the theoretical wavelength prior to shifting [λ_{theor}(Å)] is given, followed by the calculated (statistically weighted) Einstein coefficient for spontaneous emission of the transition (gA), and the total (statistically weighted) coefficient for autoionization from the upper level of the transition (ΣgA^a) obtained by summing over all possible autoionization channels. g denotes the statistical weight of the upper level. The next column displays the identified radiative transition. For the upper level of the transition, only the most important components of the eigenvector are given, preceded by the square of their coefficients. The last two columns show the total angular momentum of the lower (J_L) and upper (J_U) levels of the transition. Tentative identifications are marked by a. It is worth noting that, in general, the observed spectral peaks are not necessarily individual lines and still may include a few blended lines. Some peaks, on the other hand, are found to be pure single Cu-like lines, e.g., peaks 9 and 11. In the following, these two lines will prove to be suitable for electron density diagnostics.

V. PLASMA DIAGNOSTICS

A. Electron density

One specific pair of lines for which the intensity ratio is sufficiently sensitive to the electron density is found to be the pair of lines 9 and 11 (see Fig. 3) emitted by Cu-like barium. These two lines arise from $3d^{10}4l$-$3d^9 4l6f$ transitions; line 9 with a $4p$ electron spectator, and line 11 with a $4s$ spectator. Figure 4 gives the calculated intensity ratio for the two lines as a function of the electron density for a temperature of 120 eV, which corresponds to the present experiment as indicated in Sec. V B. It can be seen that this intensity ratio significantly varies in the 10^{19}–10^{22}-cm^{-3} electron density range from about 40 to 2, and thus can be used for diagnostics in this range. The reason for the high sensitivity of the intensity ratio is that there is a large difference between the autoionization rates of the upper levels of the two transitions, while the radiative rates are comparable, as indicated in Table I. Line 11 is already strong at low electron density due to intense dielectronic capture, which is proportional to the autoionization coefficient ($gA^a=1.91\times10^{13}$ s^{-1}). Line 9, on the other hand, is weak at low density ($gA^a=7.44\times10^{11}$ s^{-1}) and becomes intense only when collisional processes between doubly excited levels start being significant and strongly populate the upper level of the transition. The intensity ratio measured in the present experiment is around 2.2 and is represented in Fig. 4 by the horizontal bars, which show the experimental error. It can be seen from the figure that this measurement indicates a density of at least 3×10^{21} cm^{-3} but not higher than 10^{23} cm^{-3}.

The above diagnosis gives mainly a clear lower limit, but not a very good upper limit, for the electron density. In order to better evaluate the upper density limit, several other density-dependent line intensities in the theoretical Cu-like spectra have been examined. The intensity ratios of these additional lines are less sensitive to the electron density for $n_e<10^{21}$ cm^{-3}, but are somewhat more sensitive in the limited 10^{21}–10^{23}-cm^{-3} range than the pair of lines used in Fig. 4. The overall analysis of these additional results enables a more accurate upper limit estimation for the electron density found here to be 8×10^{21} cm^{-3}. To summarize, the electron density here is estimated to be between 3×10^{21} and 8×10^{21} cm^{-3}. For the purpose of the further calculations, the value of the electron density is henceforth taken to be 5×10^{21} cm^{-3}. It should be stressed that since the analyzed spectrum is space and time integrated, the value 5×10^{21} cm^{-3} actually represents the density spatially averaged over the Cu-like $3d$-$6f$ emitting region of the plasma, and temporally averaged over the duration of this emission.

B. Electron temperature

One expects difficulties in finding a particular pair of lines of the same ionization state in the limited spectral region of the present experiment for which the intensity ratio is very

TABLE I. Experimental and theoretical line wavelengths in the 9.10–9.36-Å range and the corresponding identified Cu-, Zn-, and Ga-like barium transitions. For the upper level of the transitions, the most important components of the eigenvector are given, preceded by the square of their coefficients. Labels refer to the peaks of the experimental spectrum in Fig. 3. gA and ΣgA^a represent the statistically weighted Einstein coefficients for spontaneous emission and the sum of the coefficients for autoionization from the upper level, respectively; $X(Y)$ stands for $X\times10^Y$. J_L and J_U are the total angular momenta of the lower and upper levels, respectively.

Label	λ_{expt} (Å)	Ion (sequence)	λ_{theor} (Å)	gA (s^{-1})	ΣgA^a (s^{-1})	Transition	J_L	J_U
1	9.1428	Ba^{27+}(Cu I)	9.156	5.84(13)	9.42(11)	$3d^{10}4p$ - $72\%(3d^9_{3/2}4p_{3/2})_1 6f_{5/2}$	3/2	5/2
		Ba^{27+}(Cu I)	9.158	3.78(13)	2.53(11)	$3d^{10}4p$ - $76\%(3d^9_{3/2}4p_{3/2})_2 6f_{5/2}$	3/2	3/2
		Ba^{27+}(Cu I)	9.160	7.79(13)	3.66(14)	$3d^{10}4d$ - $59\%(3d^9_{3/2}4d_{5/2})_3 6f_{5/2}$	5/2	7/2
2	9.1491	Ba^{27+}(Cu I)	9.164	2.44(13)	1.19(13)	$3d^{10}4s$ - $96\%(3d^9_{3/2}4s)_2 6f_{5/2}$	1/2	1/2
		Ba^{27+}(Cu I)	9.165	3.90(13)	4.60(11)	$3d^{10}4p$ - $69\%(3d^9_{3/2}4p_{1/2})_1 6f_{5/2}$	1/2	3/2
3	9.1518	Ba^{27+}(Cu I)	9.166	4.72(13)	3.43(13)	$3d^{10}4s$ - $55\%(3d^9_{3/2}4s)_2 6f_{5/2}$	1/2	3/2
4	9.1578	Ba^{27+}(Cu I)	9.171	2.36(13)	2.98(13)	$3d^{10}4p$ - $90\%(3d^9_{3/2}4p_{1/2})_2 6f_{5/2}$	1/2	1/2
5	9.1622	Ba^{27+}(Cu I)[a]	9.179	2.55(13)	1.66(14)	$3d^{10}4d$ - $44\%(3d^9_{3/2}4d_{3/2})_3 6f_{5/2}$ + $38\%(3d^9_{3/2}4d_{3/2})_1 6f_{5/2}$	3/2	5/2
6	9.1749	Ba^{27+}(Cu I)	9.207	7.32(12)	7.68(12)	$3p^6 3d^{10}4p$ - $99\%(3p^5_{3/2}3d^{10}4p_{3/2})_3 5s$	3/2	5/2
		Ba^{27+}(Cu I)	9.209	5.16(12)	2.65(12)	$3p^6 3d^{10}4p$ - $95\%(3p^5_{3/2}3d^{10}4p_{1/2})_2 5s$	1/2	3/2
		Ba^{27+}(Cu I)	9.209	2.64(12)	2.86(10)	$3p^6 3d^{10}4s$ - $100\%(3p^5_{3/2}3d^{10}4s)_1 5s$	1/2	1/2
7	9.1845	Ba^{25+}(Ga I)[a]	9.154	2.12(13)	2.97(13)	$3d^{10}4s^2 4p$ - $67\%(3d^9_{5/2}4s^2 4p_{3/2})_3 7f_{7/2}$	3/2	5/2
8	9.1901	Ba^{25+}(Ga I)	9.163	2.84(13)	1.72(13)	$(3d^{10}4s4p_{1/2})_1 4p_{3/2}$ - $34\%([(3d^9_{5/2}4s)_2 4p_{1/2}]_{3/2}4p_{3/2})_0 7f_{7/2}$ + $19\%([(3d^9_{5/2}4s)_2 4p_{1/2}]_{3/2}4p_{3/2})_1 7f_{7/2}$	5/2	7/2
		Ba^{25+}(Ga I)	9.170	1.03(13)	2.30(13)	$3d^{10}4s^2 4p$ - $92\%(3d^9_{5/2}4s^2 4p_{1/2})_3 7f_{7/2}$	1/2	1/2
		Ba^{25+}(Ga I)	9.172	1.98(13)	2.74(13)	$3d^{10}4s^2 4p$ - $53\%(3d^9_{5/2}4s^2 4p_{1/2})_3 7f_{7/2}$	1/2	3/2
		Ba^{25+}(Ga I)	9.174	1.95(13)	2.54(13)	$3d^{10}4s4p^2_{1/2}$ - $65\%(3d^9_{5/2}4s)_2(4p^2_{1/2})_0 7f_{7/2}$	1/2	3/2
9	9.2472	Ba^{27+}(Cu I)	9.261	3.88(13)	7.44(11)	$3d^{10}4p$ - $53\%(3d^9_{5/2}4p_{3/2})_3 6f_{7/2}$	3/2	5/2
10	9.2554	Ba^{27+}(Cu I)[a]	9.266	2.08(13)	1.15(10)	$3d^{10}4p$ - $87\%(3d^9_{5/2}4p_{3/2})_3 6f_{7/2}$	3/2	3/2
		Ba^{27+}(Cu I)[a]	9.267	3.62(13)	1.70(14)	$3d^{10}4d$ - $42\%(3d^9_{5/2}4d_{5/2})_4 6f_{7/2}$ + $33\%(3d^9_{5/2}4d_{5/2})_2 6f_{7/2}$	5/2	7/2
11	9.2601	Ba^{27+}(Cu I)	9.273	3.20(13)	1.91(13)	$3d^{10}4s$ - $65\%(3d^9_{5/2}4s)_2 6f_{7/2}$	1/2	3/2
12	9.2640	Ba^{27+}(Cu I)	9.277	3.26(13)	9.72(12)	$3d^{10}4p$ - $43\%(3d^9_{5/2}4p_{1/2})_2 6f_{7/2}$ + $43\%(3d^9_{5/2}4p_{1/2})_3 6f_{7/2}$	1/2	3/2
		Ba^{27+}(Cu I)	9.278	1.62(13)	1.55(13)	$3d^{10}4s$ - $88\%(3d^9_{5/2}4s)_3 6f_{7/2}$	1/2	1/2
13	9.3295	Ba^{26+}(Zn I)	9.347	3.76(13)	1.51(13)	$3d^{10}4s4p_{3/2}$ - $61\%[(3d^9_{3/2}4s)_2 4p_{3/2}]_{3/2}6f_{5/2}$	1	2
14	9.3345	Ba^{26+}(Zn I)	9.353	3.00(13)	1.55(13)	$3d^{10}4s4p_{3/2}$ - $39\%[(3d^9_{3/2}4s)_2 4p_{3/2}]_{3/2}6f_{5/2}$ + $19\%[(3d^9_{3/2}4s)_1 4p_{3/2}]_{5/2}6f_{5/2}$	1	1
15	9.3428	Ba^{26+}(Zn I)	9.358	5.67(13)	8.12(12)	$3d^{10}4p^2_{3/2}$ - $35\%[3d^9_{3/2}(4p^2_{3/2})_2]_{5/2}6f_{5/2}$ + $13\%[3d^9_{3/2}(4p^2_{3/2})_2]_{7/2}6f_{5/2}$	2	3
		Ba^{26+}(ZnI)	9.358	5.15(13)	2.23(13)	$3d^{10}4p_{1/2}4p_{3/2}$ - $43\%[(3d^9_{3/2}4p_{1/2})_1 4p_{3/2}]_{3/2}6f_{5/2}$ + $13\%[(3d^9_{3/2}4p_{1/2})_2 4p_{3/2}]_{5/2}6f_{5/2}$	2	3
16	9.3509	Ba^{26+}(Zn I)	9.361	3.25(13)	3.72(13)	$3d^{10}4s4p_{3/2}$ - $69\%[(3d^9_{3/2}4s)_2 4p_{3/2}]_{7/2}6f_{5/2}$	2	1
		Ba^{26+}(Zn I)	9.361	6.60(13)	3.05(13)	$3d^{10}4s4p_{3/2}$ - $30\%[(3d^9_{3/2}4s)_2 4p_{3/2}]_{5/2}6f_{5/2}$ + $29\%[(3d^9_{3/2}4s)_1 4p_{3/2}]_{5/2}6f_{5/2}$	2	3
		Ba^{26+}(Zn I)	9.362	4.86(13)	1.90(13)	$3d^{10}4s4p_{3/2}$ - $35\%[(3d^9_{3/2}4s)_2 4p_{3/2}]_{5/2}6f_{5/2}$ + $29\%[(3d^9_{3/2}4s)_1 4p_{3/2}]_{5/2}6f_{5/2}$	2	2

[a]Tentative identification.

sensitive to the electron temperature. This is due to the narrow energy spread of the doubly excited levels from which the present spectrum is emitted. Thus, in order to estimate the electron temperature, the temperature dependence of the detailed features in the calculated spectrum are systematically analyzed. Figure 5 gives the theoretical results of the model (thin traces) for three different electron temperatures at a fixed electron density of 5×10^{21} cm^{-3}, each compared to the experimental spectrum (thick traces). By closely examining the theoretical and experimental spectra, and in particular the relative intensities of lines 2 and 3, and those of lines 11 and 12, it can be seen that the theoretical spectrum in Fig. 5(b) agrees with the experimental results better than the other two. A more accurate determination of the temperature is achieved by carefully comparing various calculated spectra for temperatures closer to 100 eV. Finally, the electron temperature for which the best fit to experiment is obtained is 120 eV. This temperature evaluation is estimated to be accurate to about ±30 eV. As for the electron density, the evaluated electron temperature here represents the mean tem-

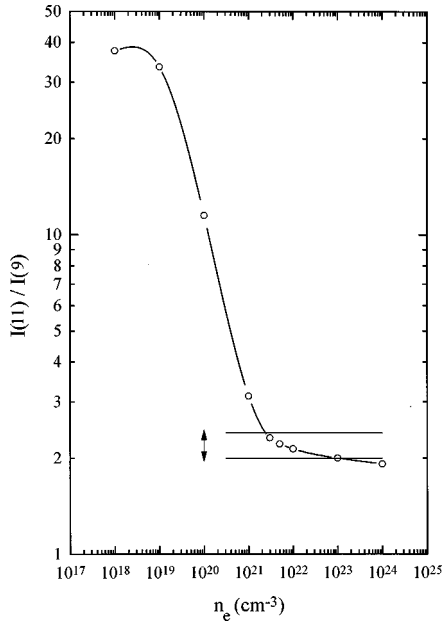

FIG. 4. Density-sensitive intensity ratio of the Cu-like barium lines 11 and 9 calculated for $kT_e = 120$ eV. The curve connects the calculated values (hollow circles). The horizontal bars define the experimental intensity ratio measurement.

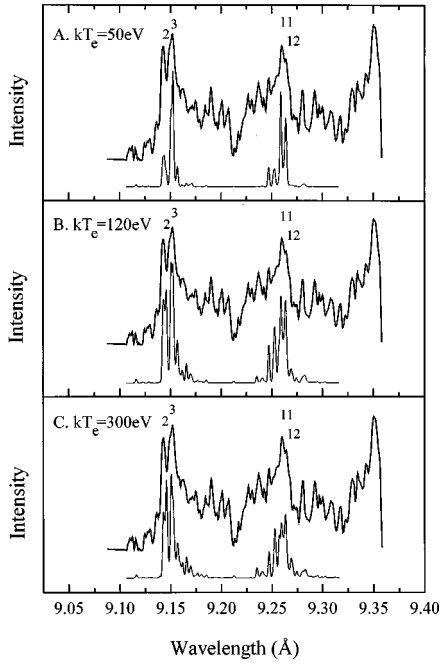

FIG. 5. Theoretical spectra (thin traces) of the $3d^{10}4l$-$3d^{9}4l6f$ Cu-like barium transitions for three different electron temperatures: 50 eV (a), 120 eV (b), and 300 eV (c) for an electron density of 5×10^{21} cm^{-3} compared to the experimental spectrum (thick traces).

perature for the region and duration of the Cu-like $3d$-$6f$ emission. It should be pointed out that this temperature corresponds to an average energy much below the ionization energy of the ions. For instance, the calculated ionization energies of Cu- and Zn-like barium are 975 and 935 eV, respectively.

It is not unusual to find highly ionized laboratory plasmas at electron temperatures corresponding to energies much lower than the ionization energies of the ions present in the plasma. This situation was explained in very dense plasmas approaching LTE conditions [2] (opposite to low-density non-LTE steady-state plasmas where the maximum abundance for a given ionization state occurs at a higher electron temperature than in LTE). However, in the present experiment we are not in this high-density regime. In still other experiments, this situation can be explained by the existence of highly energetic electrons (several keV) that are capable of ionizing the atoms up to very high ionization states [15,16]. In the present case, irrespective of how the highly ionized atoms are formed, we suggest that the major portion of photons in the recorded spectrum are emitted during the transient expanding phase, while the plasma is cooling and recombination processes dominate. Indeed, at $n_e = 5\times10^{21}$ cm^{-3} and $kT_e = 120$ eV the present collisional-radiative model predicts that essentially all of the doubly excited levels are populated by dielectronic capture, since the temperature is too low for inner-shell excitation to be efficient. The effect of multistep excitation to the high doubly excited levels has also been checked and found to be negligible at the present temperature and density.

The intensity of almost pure dielectronic recombination Cu-like lines, such as that of the present spectrum, is approximately proportional to the abundance of Ni-like ions. From the Saha equation we would expect the abundance of Ni-like barium ions to be substantial (e.g., $n_{\mathrm{Ni\,I}} \approx n_{\mathrm{Cu\,I}}$) in a 5×10^{21} cm^{-3} LTE plasma only at an electron temperature of about 200 eV and higher. Therefore, as has been assumed here, the plasma region emitting Cu-like lines, which is found to be at 120 eV, clearly departs from pure steady-state LTE conditions. The present spectrum, hence, reflects the transient cooling phase of the recombining and expanding plasma. Fast electrons are assumed to have already disappeared from the plasma at this late stage. In addition, calculations show that electrons of a few keV are not expected to influence the general shape of the present spectrum.

C. Dependence on fractional ion abundances

In general, the spectrum emitted by a plasma composed of several ionization states is expected to be dependent on the fractional ion abundances. Moreover, in transient non-LTE plasmas with strong temperature and density gradients, these abundances are space and time dependent and are not easily determined. The straightforward approach for estimating the fractional abundances by comparing intensities of spectral lines from adjacent ionization states cannot be used for lines emitted from doubly excited autoionizing levels, since the intensities of these lines also depend on the abundance of the ions in the next ionization state.

Fortunately, in the case of relatively low electron temperature, as in the present plasma ($kT_e < 300$ eV), the spectrum of (Cu-like) doubly excited ions almost purely originates from dielectronic capture processes (Sec. V B), and not from inner-shell excitations from low levels, which require very high incident electron energies. Thus, the doubly excited ion density n_d is proportional to the ion density of the next ionization state (Ni-like). Consequently, the *relative* intensities of the dielectronic recombination lines *within* each

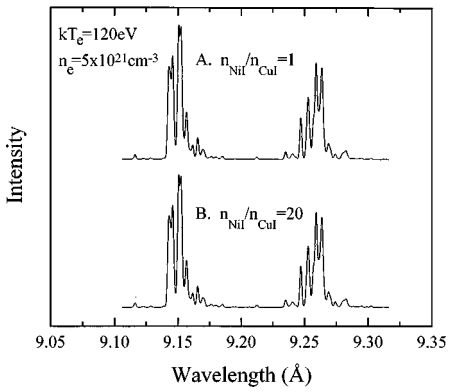

FIG. 6. Similar theoretical spectra of the $3d^{10}4l$-$3d^{9}4l6f$ Cu-like barium transitions obtained for two different ionization balance conditions for the Ni- and Cu-like ions: $n_{\mathrm{Ni\,I}}/n_{\mathrm{Cu\,I}}=1$ (a) and $n_{\mathrm{Ni\,I}}/n_{\mathrm{Cu\,I}}=20$ (b), both at an electron temperature of 120 eV and an electron density of 5×10^{21} cm^{-3}.

ionization state are independent of the ion density ratio of the adjacent ionization states. This result is illustrated in Fig. 6, where the theoretical spectrum of Cu-like barium in the considered wavelength range is shown for two very different values of the $n_{\mathrm{Ni\,I}}/n_{\mathrm{Cu\,I}}$ ratio at a fixed low temperature of 120 eV and a fixed density of 5×10^{21} cm^{-3}. The two spectra, for $n_{\mathrm{Ni\,I}}/n_{\mathrm{Cu\,I}}=1$ [Fig. 6(a)] and for $n_{\mathrm{Ni\,I}}/n_{\mathrm{Cu\,I}}=20$ [Fig. 6(b)], are found to be almost identical. The same result is obtained at this temperature for other densities as well.

The fact that the relative line intensities are not dependent upon the $n_{\mathrm{Ni\,I}}/n_{\mathrm{Cu\,I}}$ ratio is not necessarily true at high electron temperatures where inner-shell excitations become significant. In particular, at low electron density, the relative line intensities vary drastically as a function of the $n_{\mathrm{Ni\,I}}/n_{\mathrm{Cu\,I}}$ ratio. This feature can be seen in Figs. 7(a) and 7(b), which present the spectrum emitted by Cu-like barium at a fixed high temperature of 700 eV and a fixed low density of 10^{16} cm^{-3}, for $n_{\mathrm{Ni\,I}}/n_{\mathrm{Cu\,I}}=1$ [Fig. 7(a)] and for $n_{\mathrm{Ni\,I}}/n_{\mathrm{Cu\,I}}=20$ [Fig. 7(b)]. In contrast, at higher densities, the collisional transitions between the doubly excited states become efficient and predominantly determine the relative populations of the doubly excited levels, regardless of whether they were initially populated by dielectronic capture, or by inner-shell excitation. This effect can be seen in Figs. 7(c) and 7(d), which show similar spectra for the two different abundance ratios.

In conclusion, in the relatively low temperature and high electron density regime of the present experiment, the relative line intensities emitted by each ionization species are not sensitive to the fractional ion abundances; consequently, they cannot be used to derive even the average ionization balance of the plasma.

VI. CONCLUSION

The x-ray spectrum emitted by a highly stripped laser-produced barium plasma has been recorded with very high spectral resolution using a spherically bent mica crystal. An elaborate level-by-level collisional-radiative model including autoionization and dielectronic capture processes has been constructed for identifying the newly resolved spectral features and for performing new diagnostics of the plasma parameters. New $3d$-nf ($n=6,7$) and $3p$-$5s$ spectral lines have been identified. The measured relative line intensities are used to deduce the time and space averaged electron density and temperature of the plasma region emitting these lines. The best fit between theory and experiment for the Cu-like spectrum is obtained for approximately 5×10^{21} cm^{-3} and 120 eV, respectively. This low electron temperature can be explained by assuming that the spectrum is emitted from the expanding plasma during its late phase when cooling takes place and dielectronic recombination dominates.

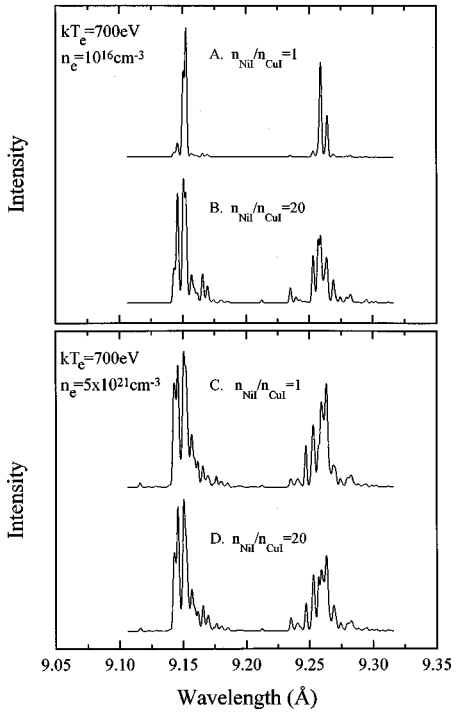

FIG. 7. Theoretical spectra of the $3d^{10}4l$-$3d^{9}4l6f$ Cu-like barium transitions for an electron temperature of 700 eV. Plots (a) and (b) are for an electron density of 10^{16} cm^{-3} at two different ionization balance conditions: $n_{\mathrm{Ni\,I}}/n_{\mathrm{Cu\,I}}=1$ (a) and $n_{\mathrm{Ni\,I}}/n_{\mathrm{Cu\,I}}=20$ (b). Plots (c) and (d) are for an electron density of 5×10^{21} cm^{-3}, for the two ion abundance ratios.

It has been found that at the low temperature of 120 eV, collisional inner-shell excitations are not significant, and therefore the dielectronic capture processes govern the population distribution among the doubly excited levels. As a result, the relative line intensities in the limited wavelength region investigated here are independent of the fractional ion abundances. Further investigations using time and space resolved measurement techniques are needed to give deeper insight into the mechanisms responsible for the evolution of level populations and ion state abundances in subpicosecond laser-produced plasmas.

ACKNOWLEDGMENTS

E.B. was supported by The Charles Clore Israel Foundation. A.Y.F. and T.A.P. were supported in part by The Russian Fundamental Science Foundation under Grant No. 96-02-16111.

[1] A. Zigler, P. G. Burkhalter, D. J. Nagel, M. D. Rosen, K. Boyer, G. Gibson, T. S. Luk, A. McPherson, and C. K. Rhodes, Appl. Phys. Lett. **59**, 777 (1991).
[2] W. H. Goldstein, A. Zigler, P. G. Burkhalter, D. J. Nagel, A. Bar-Shalom, J. Oreg, T. S. Luk, A. McPherson, and C. K. Rhodes, Phys. Rev. E **47**, 4349 (1993).
[3] R. Doron, M. Fraenkel, P. Mandelbaum, A. Zigler, and J. L. Schwob, Phys. Scr. **58**, 19 (1998).
[4] A. Ya. Faenov, S. A. Pikuz, A. I. Erko, B. A. Bryunetkin, V. M. Dyakin, G. V. Ivaneko, A. R. Mingleev, T. A. Pikuz, V. M. Romanova, and T. A. Shelkovenko, Phys. Scr. **50**, 333 (1994).
[5] A. Ya. Faenov, B. A. Bryunetkin, V. M. Dyakin, T. A. Pikuz, I. Yu. Skobelev, S. A. Pikuz, J. Nilsen, A. L. Osterheld, and U. I. Safronova, Phys. Rev. A **52**, 3644 (1995).
[6] J. P. Geindre, P. Audebert, A. Rousse, J. C. Gauthier, A. Ya. Faenov, S. A. Pikuz, T. A. Pikuz, and T. A. Shelkovenko, Phys. Scr. **53**, 645 (1996).
[7] A. Bar-Shalom, J. Oreg, W. H. Goldstein, D. Shvarts, and A. Zigler, Phys. Rev. A **40**, 3183 (1989).
[8] C. Bauche-Arnoult, J. Bauche, E. Luc-Koenig, J. F. Wyart, R. M. More, C. Chenais-Popovics, J. C. Gauthier, J. P. Geindre, and N. Tragin, Phys. Rev. A **39**, 1053 (1989).
[9] P. Mandelbaum, D. Mitnik, E. Behar, R. Doron, and J. L. Schwob, J. Quant. Spectrosc. Radiat. Transf. **54**, 261 (1995).
[10] G. Mourou and D. Umstadter, Phys. Fluids B **4**, 2315 (1992).
[11] P. D. Rockett, C. R. Bird, C. J. Hailey, D. Sullivan, D. B. Brown, and P. G. Burkhalter, Appl. Opt. **24**, 2536 (1985).
[12] B. L. Henke and P. A. Jaanimagi, Rev. Sci. Instrum. **56**, 1537 (1985).
[13] A. Bar-Shalom, M. Klapisch, and W. H. Goldstein, the HULLAC code for atomic physics (1988) (unpublished).
[14] M. Klapisch, Comput. Phys. Commun. **2**, 239 (1971).
[15] A. Rousse, P. Audebert, J. P. Geindre, F. Falliès, J. C. Gauthier, A. Mysyrowicz, G. Grillon, and A. Antonetti, Phys. Rev. E **50**, 2200 (1994).
[16] F. B. Rosmej, B. A. Bryunetkin, A. Ya. Faenov, I. Yu. Skobelev, M. P. Kalashnikov, P. V. Nickles, and M. Schnurer, J. Phys. B **29**, L299 (1996).